



CFD modeling of
sulfur driven
nucleation and
growth in diluting
diesel exhaust

M. Olin et al.

CFD modeling of a vehicle exhaust laboratory sampling system: sulfur driven nucleation and growth in diluting diesel exhaust

M. Olin, T. Rönkkö, and M. Dal Maso

Aerosol Physics Laboratory, Department of Physics, Tampere University of Technology, P.O. Box 692, 33101 Tampere, Finland

Received: 12 November 2014 – Accepted: 2 January 2015 – Published: 29 January 2015

Correspondence to: M. Olin (miska.olin@tut.fi)

Published by Copernicus Publications on behalf of the European Geosciences Union.

Title Page

Abstract

Introduction

Conclusions

References

Tables

Figures



Back

Close

Full Screen / Esc

Printer-friendly Version

Interactive Discussion



Abstract

A new exhaust aerosol model CFD-TUTEAM (Tampere University of Technology Exhaust Aerosol Model for Computational Fluid Dynamics) was developed. The model can be used to simulate particle formation and evolution in diesel exhaust. The model has an Eulerian sub-model that provides spatial information within the computational domain, and a computationally less expensive Lagrangian sub-model that can be used to examine particle formation in a high temporal resolution. Particle formation in a laboratory sampling system that includes a porous tube type diluter and an aging chamber was modeled with CFD-TUTEAM. The simulation results imply that over 99 % of new particles are formed in the aging chamber region, because nucleation rate remains at high level in the aging chamber due to low dilution ratio and low nucleation exponents. The nucleation exponents for sulfuric acid in sulfuric acid-water nucleation ranging from 0.25 to 1 appeared to fit best with measurement data, which are the same values as the slopes of volatile nucleation mode number concentration vs. raw exhaust sulfuric acid concentration obtained from the measurement data. These nucleation exponents are very low compared to the nucleation exponents obtained from the classical nucleation theory of binary sulfuric acid-water nucleation. The values of nucleation exponent lower than unity suggest that other compounds, such as hydrocarbons, might have a significant role in the nucleation process.

1 Introduction

Ultrafine particles are related to adverse health effects (Dockery et al., 1993; Pope et al., 2002; Beelen et al., 2014) and various effects on climate (Arneth et al., 2009). Diesel vehicles have a significant role on the health effects, because they have a major contribution to ultrafine particles of urban air (Virtanen et al., 2006; Johansson et al., 2007; Pey et al., 2009) and because the sizes of the particles emitted by diesel vehicles

ACPD

15, 2905–2956, 2015

CFD modeling of sulfur driven nucleation and growth in diluting diesel exhaust

M. Olin et al.

Title Page

Abstract

Introduction

Conclusions

References

Tables

Figures

◀

▶

◀

▶

Back

Close

Full Screen / Esc

Printer-friendly Version

Interactive Discussion

lie in the range of high lung deposition probability (Alföldy et al., 2009; Rissler et al., 2012).

Fuel combustion generates solid particles, such as soot, ash, core (Rönkkö et al., 2007), and nanosized carbonaceous particles (Sgro et al., 2008). In addition to solid particles, liquid particles are also formed. Unlike solid particles, liquid particles are formed after the combustion process during exhaust cooling (Kittelson, 1998). In the case of a vehicle, this occurs when the exhaust is released from the tailpipe. These particles are smaller in size than soot particles, and they are formed through nucleation process; thus they are frequently called nucleation particles. In fact, nucleation process involves an energy barrier, but particle formation can be a barrierless process also (Vehkamäki and Riipinen, 2012). For simplicity, particle formation process in this article is called nucleation process, whether it has an energy barrier or not.

Particle size distribution controls the aerosol deposition to the respiratory system and its behavior in the atmosphere. Modeling studies can provide information on vehicle exhaust particle formation and evolution in the atmosphere. To model particle concentration and the size of nucleation mode, the actual nucleation rate is required to be known. Modeling of vehicle exhaust particle formation can provide useful information on the atmospheric nucleation also.

The detailed nucleation mechanism that controls particle formation in vehicle exhaust is currently unknown. Nucleation particles are known to consist of water, sulfuric acid, and hydrocarbons (Kittelson, 1998; Tobias et al., 2001; Sakurai et al., 2003; Schneider et al., 2005), and therefore it is likely that these could be involved in nucleation process. Sulfuric acid concentration in diesel exhaust (Rönkkö et al., 2013), fuel sulfur content (Maricq et al., 2002; Vogt et al., 2003; Vaaraslahti et al., 2005; Kittelson et al., 2008), lubricating oil sulfuric content (Vaaraslahti et al., 2005; Kittelson et al., 2008), and exhaust after-treatment (Vogt et al., 2003) have been found to correlate with nucleation particle concentration, at least in the cases when the test vehicle has been equipped with an oxidative exhaust after-treatment. For an opposite example, no

CFD modeling of sulfur driven nucleation and growth in diluting diesel exhaust

M. Olin et al.

Title Page

Abstract

Introduction

Conclusions

References

Tables

Figures



Back

Close

Full Screen / Esc

Printer-friendly Version

Interactive Discussion



correlation between fuel sulfur content and particle number concentration can be seen from the results of Rönkkö et al. (2007).

Particle formation and dilution in vehicle exhaust and in laboratory sampling systems has been studied by several authors (Vouitsis et al., 2005; Lemmetty et al., 2006, 2008; Arnold et al., 2012; Li and Huang, 2012; Pirjola et al., 2014) in temporal coordinates. However, because particle formation in diluting vehicle emission involves strong gradients in temperature and the concentration of compounds involved, full understanding of the particle formation process requires also information in the spatial dimensions, usually by using a computational fluid dynamics (CFD) approach. For vehicle exhaust plumes, modeling efforts to elucidate this situation have been undertaken recently (Uhrner et al., 2007; Albriet et al., 2010; Liu et al., 2011; Wang and Zhang, 2012; Huang et al., 2014). These efforts, however, have focused on real-world dilution situations, for which boundary conditions are difficult to obtain. Controlled observations of vehicle emissions are usually performed in laboratory conditions involving diluting sampling systems. CFD modeling of particle formation in a perforated tube diluter (its operating principle corresponds to a porous tube diluter (PTD) used in exhaust laboratory measurements) with dibutylphthalate (DBP) has been performed by Pyykönen et al. (2007). To our knowledge, no CFD modeling studies involving realistic vehicle exhaust in realistic emission sampling situations have been performed.

In this paper, an exhaust aerosol model for application in CFD modeling of realistic vehicle exhaust and its applicability to study particle formation involving sulfuric acid in diesel exhaust using previously published data (Arnold et al., 2012; Rönkkö et al., 2013) are presented. Two versions of the model code, an Eulerian and a Lagrangian model, are presented. Then the model is used to examine the spatial distribution of particle formation and growth in the modeled experimental setup, the findings in light of different possible nucleation mechanisms through the dependence of the formation rate on the sulfuric acid concentration are studied. In addition it was possible to study the relative rates of different aerosol dynamical processes such as coagulation and deposition inside the sampling setup, which provides valuable information for future

CFD modeling of sulfur driven nucleation and growth in diluting diesel exhaust

M. Olin et al.

Title Page

Abstract

Introduction

Conclusions

References

Tables

Figures

◀

▶

◀

▶

Back

Close

Full Screen / Esc

Printer-friendly Version

Interactive Discussion



studies of vehicle emissions. Finally, because vehicle emission studies are used as input for modeling studies of atmospheric aerosol loading, the spatial information gained from our model gives insight into the applicability of emission studies for such upscaling purposes.

2 Model description

2.1 Fluid dynamics model

CFD code used was commercially available software ANSYS FLUENT 14.0. It can be used to solve, e.g., flow, mass, heat, and radiation transfer problems. It is based on finite volume method (ANSYS, 2011), where the computational domain is divided into finite amount of cells. Governing equations of the flow are solved in every computational cell iteratively until sufficient convergence is reached. In this case, the governing equations are continuity, momentum, energy, turbulence, gas species, and aerosol scalars transport equations.

2.2 Aerosol dynamics model CFD-TUTEAM

Aerosol dynamics model CFD-TUTEAM (Tampere University of Technology Exhaust Aerosol Model for Computational Fluid Dynamics) is based on former aerosol model TUTEAM (Lemmetty et al., 2008). CFD-TUTEAM models aerosol distributions modally (Whitby and McMurry, 1997), i.e. the total distribution is divided into log-normally distributed modes of different particle size. A single-component mode j is modeled by three variables, which are number $M_{j,0}$, surface area $M_{j,2/3}$ and mass $M_{j,1}$ moment concentrations of a distribution. The concentration of a k th moment of a mode j has a governing equation (Whitby and McMurry, 1997)

$$\frac{\partial M_{j,k}}{\partial t} = -\nabla \cdot (M_{j,k} \mathbf{u}) + \nabla \cdot \left(\rho_f \bar{D}_{j,k,\text{eff}} \nabla \frac{M_{j,k}}{\rho_f} \right) + \text{nucl}_{j,k} + \text{cond}_{j,k} + \text{coag}_{j,k}, \quad (1)$$

2909

CFD modeling of sulfur driven nucleation and growth in diluting diesel exhaust

M. Olin et al.

Title Page

Abstract

Introduction

Conclusions

References

Tables

Figures

◀

▶

◀

▶

Back

Close

Full Screen / Esc

Printer-friendly Version

Interactive Discussion



CFD modeling of sulfur driven nucleation and growth in diluting diesel exhaust

M. Olin et al.

Title Page

Abstract

Introduction

Conclusions

References

Tables

Figures

◀

▶

◀

▶

Back

Close

Full Screen / Esc

Printer-friendly Version

Interactive Discussion

where \mathbf{u} is flow velocity vector, ρ_f is fluid density, $\overline{D}_{j,k,\text{eff}}$ is k th moment-weighted average of D_{eff} , and the last terms present source terms for nucleation, condensation, and coagulation, which are described in Sect. 2.2.3. However, in multi-component aerosol system, the mass moments are further divided into moments $M_{j,1,i}$ where i denotes a liquid component in the particle.

The parameters of log-normal distributions (number concentration N_j , count median diameter CMD_j and geometric SD GSD_j) can be calculated from the three moments according to Whitby and McMurry (1997).

CFD-TUTEAM consists of an Eulerian and a Lagrangian type sub-model. In the Eulerian model, the moment variables are connected to the CFD model by solving the scalar transport equations of type Eq. (1). The Lagrangian model uses cooling and dilution profiles obtained from the CFD model as inputs.

2.2.1 Eulerian model

The Eulerian aerosol model is two-way coupled with the CFD model: (1) the properties on the fluid side affect on the transport equation of the particle variables Eq. (1), (2) nucleation and condensation on the aerosol side affect on the transport equation of gas species as negative source terms.

Temperature, gas species concentrations and particle distribution parameters in hot exhaust and cold dilution air are the boundary conditions that are used at the domain boundaries in the corresponding inlets. Computation of the CFD model and the Eulerian aerosol model provide the solution for flow and particle parameters inside the simulation domain and their values at the outlet.

The simulation domain is a two-dimensional axial symmetric geometry. A steady-state simulation is performed, where all time derivatives are zero, which provides shorter computation time.

2.2.2 Lagrangian model

The Lagrangian aerosol model is a Matlab-code in which the differential equations Eq. (1), with the exception of the first two terms (convection and diffusion), are solved numerically. The boundary conditions of temperature, gas species concentrations and particle distribution parameters are used as initial values. Temperature and gas species concentration data from different path lines of the fluid obtained from the CFD model are used as time series inputs for the Lagrangian model. The Lagrangian aerosol model is only one-way coupled with the CFD model, but the influence of nucleation and condensation on the properties on the fluid side is negligible.

The calculation of the Lagrangian aerosol model provides the particle distribution parameters as a function of time for different path lines. The values at the ends of the different path lines can be averaged to get information on the particle parameters at the outlet.

There is no spatial information at the path lines in the Lagrangian model, but temporal information exists. However, the Lagrangian model is also considered as steady-state simulation because the inputs are obtained from a steady-state CFD simulation. Due to fewer dimensions in Lagrangian model compared to the Eulerian model, a very high temporal resolution can be simulated. That can be used to ensure the sufficiency of spatial resolution of the computational grid of the Eulerian model by comparing the results from both models.

2.2.3 Aerosol dynamics

Modeled aerosol processes are shown in Fig. 2, and different terms of Eq. (1) are explained next.

“Nucleation” is a key process controlling particle number concentration in diluting exhaust is particle formation, which is generally considered sulfur-driven. Binary homogeneous nucleation (BHN) of water and sulfuric acid has been used as a nucleation mechanism in previous diesel exhaust modeling studies (Lemmetty et al., 2006, 2008;

CFD modeling of sulfur driven nucleation and growth in diluting diesel exhaust

M. Olin et al.

Title Page

Abstract

Introduction

Conclusions

References

Tables

Figures



Back

Close

Full Screen / Esc

Printer-friendly Version

Interactive Discussion



Uhrner et al., 2007; Albriet et al., 2010; Liu et al., 2011; Li and Huang, 2012; Wang and Zhang, 2012; Huang et al., 2014). The nucleation rate J of BHN can be derived from classical thermodynamics, and the theory is called classical nucleation theory (CNT). Following the first nucleation theorem (Kashchiev, 1982), the nucleation exponent for nucleating species i is defined as:

$$n_i = \frac{\partial \log J}{\partial \log C_i}, \quad (2)$$

where C_i is the concentration of species i . According to CNT, the nucleation exponent for gaseous sulfuric acid (subscript: sa) n_{sa} in vehicle exhaust is about 5 or more. In activation type nucleation (Kulmala et al., 2006), $n_{sa} = 1$, and in kinetic nucleation (McMurry and Friedlander, 1979), $n_{sa} = 2$. Nucleation exponents 1 and 2 are found to fit to atmospheric measurement results better than the values from CNT (Sihto et al., 2009), but they have not yet been widely explored in connection with diesel exhaust. The nucleation mechanism in diesel exhaust can differ from the mechanism in atmosphere due to different gas concentration and temperature range. According to our simulations with CNT nucleation (Olin et al., 2014), nucleation rate obtained from CNT needs to be corrected with a relatively large factor that decreases exponentially (correction factor $\propto [H_2SO_4]^{-6.6}$) with increasing sulfuric acid concentration (Fig. 1). This result suggests that CNT may overestimate n_{sa} with a value of 6.6. Therefore, n_{sa} in diesel exhaust could be very low. Low nucleation exponents indicate that there may be other species, such as organic compounds that also take part in the nucleation process. Paasonen et al. (2010) have modeled different nucleation mechanisms, including organic nucleation mechanisms, for background atmospheric conditions, and have observed that they correlate with measurement data better than sulfur driven nucleation in some cases. Mathis et al. (2004a) have experimentally determined that some organic compounds are capable of initiating and increasing or decreasing (depending on the functional groups) nucleation mode particles emitted by a diesel engine.

However, the actual nucleation rate, which is the rate of formation of new stable molecule clusters (Vehkamäki and Riipinen, 2012), cannot be measured directly, until

CFD modeling of sulfur driven nucleation and growth in diluting diesel exhaust

M. Olin et al.

Title Page

Abstract

Introduction

Conclusions

References

Tables

Figures

◀

▶

◀

▶

Back

Close

Full Screen / Esc

Printer-friendly Version

Interactive Discussion



recently, due to the small sizes of the clusters. The measurable quantity is the concentration of particles that are large enough for measurement devices, of which the observed nucleation rate can be estimated. Particle dynamics, such as condensation and coagulation, alter the particle distribution during the time, when newly formed clusters grow to measurable sizes. Therefore, the actual and the observed nucleation rates are unequal and their nucleation exponents can be different too.

In atmospheric modeling studies, activation and kinetic type nucleation rates have been used with the following forms (Sihto et al., 2009; Paasonen et al., 2010)

$$J_{\text{act}} = A[\text{H}_2\text{SO}_4] \quad (3)$$

$$J_{\text{kin}} = K[\text{H}_2\text{SO}_4]^2, \quad (4)$$

where A and K are activation and kinetic coefficients, respectively. The coefficients A and K are currently empirical constants fitted from experimental data in atmospheric modeling studies. Constant coefficients can be satisfactory approximations in atmospheric nucleation experiments, where temperature T and relative humidity RH remain nearly constants. In contrast, T and RH in vehicle exhaust are varying during the dilution and cooling process. Laboratory (Mathis et al., 2004b) and on-road studies (Rönkkö et al., 2006) of diesel exhaust particle emissions suggest that T and RH affect the nucleation particle concentration; thus T and RH have a role in nucleation rate. Therefore, constant coefficients cannot be used in modeling particle formation in vehicle exhaust.

Nucleation term in Eq. (1) is only related to volatile nucleation mode (subscript: vol), and for different moments it is

$$\text{nucl}_{\text{vol},0} = J$$

$$\text{nucl}_{\text{vol},2/3} = Jm^{*2/3}, \quad (5)$$

$$\text{nucl}_{\text{vol},1,i} = Jm_i^*$$

CFD modeling of sulfur driven nucleation and growth in diluting diesel exhaust

M. Olin et al.

Title Page	
Abstract	Introduction
Conclusions	References
Tables	Figures
◀	▶
◀	▶
Back	Close
Full Screen / Esc	
Printer-friendly Version	
Interactive Discussion	



where m^* is the mass of the cluster formed by nucleation and m_i^* the mass of component i in the cluster. Nucleation rate J depends on the theory used. In this case, the following nucleation scheme is used:

$$J = \frac{k_{n_{sa},n_w}}{\rho_{sa}^\circ(T)} [H_2SO_4]^{n_{sa}} [H_2O]^{n_w}, \quad (6)$$

5 where k_{n_{sa},n_w} is a proportionality constant and ρ_{sa}° is the saturation vapor pressure of sulfuric acid that can be found from Kulmala and Laaksonen (1990). In this form, the roles of T and RH have been included into the nucleation rate by an ad hoc formulation. Temperature dependency has been included through ρ_{sa}° , and it is in the divisor because increasing temperature has a decreasing effect on nucleation rate. The dependency of RH on nucleation rate is included through water concentration and the nucleation exponent of it n_w same way as for sulfuric acid. In the situation of constant T and RH, the nucleation rate Eq. (6) would reduce to a form of Eq. (3) in the case of $n_{sa} = 1$.

15 “Condensation” in the model is assumed to occur by sulfuric acid, water and hydrocarbons. Condensation term for sulfuric acid is

$$\text{cond}_{j,1,sa} = \int_{-\infty}^{\infty} \frac{\partial m_{p,j,sa}}{\partial t} \frac{dN}{d \ln d_p} d \ln d_p, \quad (7)$$

20 where $\frac{\partial m_{p,j,sa}}{\partial t}$ is the mass growth rate of single particle in mode j of diameter d_p by sulfuric acid described in Appendix A, and $\frac{dN}{d \ln d_p}$ is the density function of log-normal distribution. Because water condensation and evaporation are very fast processes for small particles in low RH (Wilck, 1998), modeling them would require very dense computational grid. Therefore, the water content in the equilibrium state of particles is computed following the approach of Uhrner et al. (2007), but with an additional iterative equilibrium checking procedure described in Appendix A. Condensation term for water

CFD modeling of sulfur driven nucleation and growth in diluting diesel exhaust

M. Olin et al.

Title Page

Abstract

Introduction

Conclusions

References

Tables

Figures

◀

▶

◀

▶

Back

Close

Full Screen / Esc

Printer-friendly Version

Interactive Discussion



becomes

$$\text{cond}_{j,1,w} = \kappa_j \frac{Y_{j,w}^{\text{eq}}}{Y_{j,sa}^{\text{eq}}} \text{cond}_{j,1,sa}, \quad (8)$$

where κ_j is a factor for water equilibrium, $Y_{j,w}^{\text{eq}}$ and $Y_{j,sa}^{\text{eq}}$ are the mass fractions of water and sulfuric acid in a particle that is in water equilibrium. Two immiscible liquid phases are considered in the particles: (1) solution of sulfuric acid and water, (2) hydrocarbon mixture. Condensation term for hydrocarbons is of the form of Eq. (7), but with an additional factor f_{hc} that is considered as the fraction of hydrocarbons able to condense at temperature T . The phase interactions and the hydrocarbon fraction are described in Appendix A. Due to the decreasing trend of temperature in the simulations of the sampling system, no evaporation process is included in the model.

“Coagulation” modeling is based on the model of Whitby and McMurry (1997). Intramodal coagulation of volatile nucleation mode and intermodal coagulation from volatile nucleation mode to the other modes are modeled (Fig. 2). The modeling of intramodal coagulation of core and soot modes and intermodal coagulation between them are neglected due to insignificance and irrelevancy of them compared to the modeled coagulation directions.

“Diffusion” is modeled as laminar and turbulent parts. The laminar diffusion coefficient for particles $D_{p,\text{lam}}$ is expressed as Stokes–Einstein relation (Hinds, 1999)

$$D_{p,\text{lam}} = \frac{k_B T C_c(d_p)}{3\pi\mu_f d_p}, \quad (9)$$

where k_B is the Boltzmann constant, C_c is the slip correction coefficient (Allen and Raabe, 1985), μ_f is the dynamic viscosity of fluid, and d_p is the particle diameter. The turbulent diffusion coefficient D_t is computed as $D_t = \nu_t / \text{Sc}_t$ where ν_t is the kinematic viscosity of fluid, and Sc_t is turbulent Schmidt number, for which the default value 0.7

CFD modeling of sulfur driven nucleation and growth in diluting diesel exhaust

M. Olin et al.

Title Page

Abstract

Introduction

Conclusions

References

Tables

Figures

◀

▶

◀

▶

Back

Close

Full Screen / Esc

Printer-friendly Version

Interactive Discussion



is used. The effective diffusion coefficient of gas species and of particles are $D_{\phi,\text{eff}} = D_{\phi,\text{lam}} + D_t$. In the Lagrangian model, diffusion is not modeled as in the Eulerian model. In this case, diffusion is seen as dilution of gas species and particles, which is modeled using the following formula:

$$M_{j,k}(t + \Delta t) = M_{j,k}(t) \frac{\text{DR}(t)}{\text{DR}(t + \Delta t)}, \quad (10)$$

where DR denotes dilution ratio. The dilution profiles are obtained from the CFD simulation.

“Deposition” onto the surfaces is assumed to occur only due to diffusion, because thermophoresis is found to have only a minor effect to deposition because of low thermal gradients. Deposition is modeled by setting all moments to zero on the walls.

3 Simulation setup

3.1 Simulated experiments

To demonstrate the applicability of the CFD-TUTEAM, we applied it to a laboratory sampling system for which data has already been published by Arnold et al. (2012) and Rönkkö et al. (2013). These experiments were chosen due to the availability of simultaneous measurements of particle number concentration, size distributions, and gas-phase sulfuric acid concentrations. The experiments were performed at the engine dynamometer for a heavy-duty diesel engine. The exhaust sampling was performed with a modified partial flow sampling system (Ntziachristos et al., 2004). It consists of PTD, an aging chamber and ejector diluters. It is used to mimic the particle formation of a real-world driving situation in a laboratory-scale measurement (Keskinen and Rönkkö, 2010).

In both measurements (Arnold et al., 2012; Rönkkö et al., 2013), gaseous sulfuric acid concentration before the sampling system and particle distribution after the

CFD modeling of sulfur driven nucleation and growth in diluting diesel exhaust

M. Olin et al.

Title Page

Abstract

Introduction

Conclusions

References

Tables

Figures

◀

▶

◀

▶

Back

Close

Full Screen / Esc

Printer-friendly Version

Interactive Discussion



CFD modeling of sulfur driven nucleation and growth in diluting diesel exhaust

M. Olin et al.

Title Page

Abstract

Introduction

Conclusions

References

Tables

Figures

◀

▶

◀

▶

Back

Close

Full Screen / Esc

Printer-friendly Version

Interactive Discussion



sampling system were measured. Both measurements were performed with the same engine with nearly the same measurement system. In the simulated measurements of Arnold et al. (2012) (indexed by A), fuel sulfur content was 6 ppm, but in the measurements of Rönkkö et al. (2013) (indexed by R), it was 36 ppm. The engine was equipped with a diesel oxidation catalyst (DOC) in both measurements, but there was a diesel particle filter (DPF) in A case and a partial diesel particle filter (pDPF) in R case. DPF reduces significantly more solid particles than pDPF. Therefore, the main differences between the results of these two experiments were slightly higher sulfuric acid concentrations in R case and the existence of solid particles in R case.

Measurements of 100 % engine load were simulated. Volatile nucleation mode concentration increased in both measurements, when sulfuric acid concentration increased over the time, though all the operation parameters remained constant.

3.2 Computational domain

The computational domain for the simulations consisted of PTD and aging chamber only. Secondary dilution, such as ejector diluters, is used to stop aerosol processes that alter the particle distribution and to obtain the conditions of the sample required for measurement devices. According to the measurements of Lyyränen et al. (2004) and Giechaskiel et al. (2009), an ejector diluter has only a minor effect on nucleation mode particle concentration. Particle distribution at the outlet of aging chamber is considered here the measured particle distribution, though the particle distribution was measured after the ejector diluters in the experiments. The axial symmetric domain is presented in Fig. 3.

The domain is divided into ~ 0.5 million computational cells, of which the major part are located inside the PTD where the smallest cells are needed due to high gradients. The smallest cells are $5\mu\text{m}$ in side lengths and are located in the beginning of the porous section, where the hot exhaust and the cold dilution air encounter.

Internal fluid is a mixture of air, water vapor, gaseous sulfuric acid, and hydrocarbon mixture. Particle scalars are within internal fluid also, but are not connected to fluid

properties. External fluid is modeled as air, insulation zone as wool, and the solid zones of the PTD and the aging chamber as steel.

3.3 Boundary conditions and simulation parameters

The boundary conditions are described in Table 1. 8 cases from Rönkkö et al. (2013) measurements and 9 cases from Arnold et al. (2012) measurements with different sulfuric acid mole fractions were simulated. For R cases, nonvolatile nucleation mode (core mode, subscript: core) and soot mode (subscript: soot) concentrations vary depending on the case. For A cases, core and soot modes were not found; and therefore, omitted from the simulations. Other parameters remain nearly constants in different cases.

Water vapor mole fraction in exhaust was calculated from the combustion reaction stoichiometry and with lambda value 1.54. Water vapor in dilution air was obtained by assuming that dilution air RH was 10%. RH was not measured, but RH = 10% can be considered an upper limit. Total hydrocarbon mole fraction (except for volatile hydrocarbons) was fitted to obtain the measured volatile nucleation mode particle sizes.

Deposition in the CFD model was implemented by setting the mole fraction at the boundary to zero for a depositing gas; for non-depositing gas, a zero flux at the boundary was implemented. Gas is considered depositing, if its saturation ratio exceeds unity at the boundary, and non-depositing otherwise. For sulfuric acid, saturation never exceeded unity in these simulations; hence zero flux was always used. In reality, dilution air cools PTD, but the cooling is not simulated here. Therefore, exhaust temperatures in the sampling pipe of PTD would then be lower and dilution air temperatures higher near the boundary where hot exhaust and cold dilution air encounter. Hence, sulfuric acid might then be condensed on the cooled inner walls of the sampling pipe of PTD. Saturation ratio of over unity for hydrocarbons was calculated as a fraction of condensing hydrocarbons f_{hc} described in Appendix A. All particles were modeled as depositing; thus all moments were set to zero on the walls.

CFD modeling of sulfur driven nucleation and growth in diluting diesel exhaust

M. Olin et al.

Title Page

Abstract

Introduction

Conclusions

References

Tables

Figures

◀

▶

◀

▶

Back

Close

Full Screen / Esc

Printer-friendly Version

Interactive Discussion



CFD modeling of sulfur driven nucleation and growth in diluting diesel exhaust

M. Olin et al.

Title Page

Abstract

Introduction

Conclusions

References

Tables

Figures

◀

▶

◀

▶

Back

Close

Full Screen / Esc

Printer-friendly Version

Interactive Discussion

For volatile nucleation mode, GSD_{vol} was let to vary between 1–2 to ensure it to remain in a reasonable range. Nucleation produces monodisperse particle distribution, of which GSD is 1, if a constant cluster size is used. The measured values of GSD_{vol} after the aging chamber were in the range of between 1.2 and 1.3. For core and soot modes, constant values $GSD_{core} = \sim 1.13$ and $GSD_{soot} = 2.16$ were used, which correspond to the measured values. Hence, the surface moments for core and soot modes could be omitted from the model. Core mode had initially $CMD_{core} = 10$ nm solid particle distribution, onto which liquids condense and coagulate. Soot mode was modeled as spherical particle distribution with a constant CMD_{soot} of 49 nm, which is CMD of the mobility diameter of soot particles. The reason for using a constant value was due to the assumption that soot particles do not grow by condensation but gases condense into empty spaces of the fractal particles (Lemmetty et al., 2008). Therefore, the mobility diameter remains constant, but the effective density increases. The value of $\rho_{soot} = 380 \text{ kg m}^{-3}$ was used as the effective density of a dry soot particle (Virtanen et al., 2002), assuming 49 nm particle with the fractal dimension of 2.5 and the primary particle diameter of 5 nm.

Due to steady-state simulations, all governing equations were Reynolds-averaged, i.e. time-averaged. The averaging of the momentum transport equations causes additional terms, called Reynolds stresses, to appear. Turbulence models are used to model the Reynolds stresses, but the calibration of the turbulence models have been done with experimental data, and the calibration may not be suitable in cases with different geometries, fluid mixture, and boundary conditions. In this case, SST- $k-\omega$ with Low-Re correction (ANSYS, 2011) was used as a turbulence model. It produced the most reliable results of the available turbulence models using Reynolds stresses, according to pressure drop during the porous section. Modeled turbulence levels have, however, high influence on the results, mainly on the deposition rates: overestimated turbulence level will overestimate deposition rates and the output particle concentrations will be underestimated. Particle concentration measurements in both boundaries of the simulation domain would have provided advantageous information on validating

the turbulence model for this case, but that kind of measurement has not yet been done. Enhanced turbulence models, such as Large Eddy Simulation (LES) or Direct Numerical Simulation (DNS), could produce more reliable results, but the computational cost of them is significantly higher compared to Reynolds stress models.

All cases were simulated with two nucleation exponents for sulfuric acid: $n_{sa} = 0.25$ and $n_{sa} = 1$. Relatively low nucleation exponents were chosen due to our findings (Olin et al., 2014) that imply that the nucleation exponents obtained from CNT are too high. Nucleation exponent for water vapor n_w was assumed unity in all cases, due to the lack of detailed information on that. Therefore, the nucleation rates used were the following:

$$J = \frac{5.01 \times 10^{-15} \text{ Pa cm}^{0.75} \text{ s}^{-1}}{p_{sa}^{\circ}(T)} [\text{H}_2\text{SO}_4]^{0.25} [\text{H}_2\text{O}] \quad (11)$$

$$J = \frac{7.63 \times 10^{-23} \text{ Pa cm}^3 \text{ s}^{-1}}{p_{sa}^{\circ}(T)} [\text{H}_2\text{SO}_4][\text{H}_2\text{O}], \quad (12)$$

where the units are $\text{cm}^{-3} \text{ s}^{-1}$, Pa and cm^{-3} for nucleation rate, vapor pressure and concentrations, respectively. The proportionality constants were chosen by fitting the simulated particle concentrations with the measured ones. According to the first nucleation theorem (Kashchiev, 1982), the composition of the critical cluster is connected to the nucleation exponents. However, the composition of a newly formed particle did not follow the first nucleation theorem in this case, because, firstly, nucleation exponents lower than unity would lead to a cluster containing indiscrete amount of molecules. Secondly, the critical cluster composition and nucleation exponents have recently been found to be unconnected (Kupiainen-Määttä et al., 2014). Therefore, the newly formed particle was chosen to be defined as a particle with a diameter of 1.5 nm, which is a relevant size of a particle from which atmospheric aerosol formation starts (Kulmala et al., 2007). A particle of that size would have 15 sulfuric acid and 20 water molecules to remain in water equilibrium in temperature of 100 °C and RH of 10%. Hence, the

CFD modeling of sulfur driven nucleation and growth in diluting diesel exhaust

M. Olin et al.

Title Page

Abstract

Introduction

Conclusions

References

Tables

Figures

◀

▶

◀

▶

Back

Close

Full Screen / Esc

Printer-friendly Version

Interactive Discussion



cluster formed by nucleation had the following masses of the components:

$$m_{sa}^* = 15 \times \frac{98.079 \text{ g mol}^{-1}}{N_A}$$
$$m_w^* = 20 \times \frac{18.015 \text{ g mol}^{-1}}{N_A}, \quad (13)$$

where N_A is the Avogadro constant.

4 Results and discussion

4.1 Spatial examination of particle formation in the sampling system

Figures 4 and 5 show that nucleation begins at the boundary of hot exhaust and cold dilution air. With higher nucleation exponent n_{sa} , nucleation rate reaches higher maximum values, but it diminishes faster. Due to low nucleation exponents and low dilution ratio $DR = 12$, nucleation rate remains high in the aging chamber, where the dilution process has already finished. According to the simulations, over 99 % of particles were formed in the aging chamber in all cases, which can be seen from Fig. 6 where the volatile nucleation mode concentration increases during the aging chamber.

In R cases, volatile nucleation mode number concentration was decreased 3–9 % due to coagulation, depending on the case. Cases with smallest particles had the highest coagulation losses due to increased coagulation coefficient. Coagulation to soot mode contributed over 70 % of the total coagulation loss. Deposition onto the inner surfaces of PTD and aging chamber decreased volatile nucleation mode concentration 8–14 %, depending on the case. Cases with smallest particles had also the highest deposition losses due to increased diffusion coefficient. About 25 % of core and soot particles were deposited. The fraction of the deposited particles was lower for volatile nucleation mode, because the major depositing region is the expander in the begin-

ning of the aging chamber due to increased turbulence, where only a small fraction of volatile nucleation mode particles was already formed.

Figures 7 and 8 present CMD for volatile and nonvolatile nucleation modes in the aging chamber region. CMD_{vol} at the outlet in R cases was obtained by fitting simulated and measured diameters of average volume with the amount of hydrocarbons in raw exhaust. Values of CMD_{vol} are about 1 nm lower than measured (Fig. 9), because modeled GSD_{vol} values are higher (around 1.5) than measured (below 1.3). The error is probably caused by simultaneous nucleation and condensation processes, which both account in volatile nucleation mode distribution that is modeled as log-normal in this model. In reality, the distribution will not remain log-normal when nucleation and condensation occur simultaneously.

Modeled values of CMD_{core} are about 4 nm higher than measured. This could be due to underestimated solid core particle size or underestimated condensation. Particle distribution was not measured after the aging chamber, but after the ejector diluters that were omitted from the model. Because particle sizes can, in principle, increase also in ejector diluters, CMD_{core} might be higher, if ejector diluters are modeled. However, CMD_{vol} would increase then, but not with as fast growth rate as CMD_{core} , due to smaller particle size.

The required hydrocarbon amount is also shown in Fig. 9, from which it can be seen that increased amount of hydrocarbons was required with increasing sulfuric acid amount. This is in correspondence with the observation of Arnold et al. (2012): the amount of acidic gases other than sulfuric acid correlates with the amount of sulfuric acid. These acidic gases are mainly organic gases that have lower saturation vapor pressures compared to alkanes. Due to increased amount of low-volatile hydrocarbons, the fraction of condensing hydrocarbons would be increased, but because the change of the composition of hydrocarbon mixture was not modeled, higher total hydrocarbon amount was required. For A cases, a constant value of 3 ppmC_1 was used for hydrocarbon amount, which produced CMD_{vol} values between 4.8 and 5.2 nm.

CFD modeling of sulfur driven nucleation and growth in diluting diesel exhaust

M. Olin et al.

Title Page

Abstract

Introduction

Conclusions

References

Tables

Figures

◀

▶

◀

▶

Back

Close

Full Screen / Esc

Printer-friendly Version

Interactive Discussion



CFD modeling of sulfur driven nucleation and growth in diluting diesel exhaust

M. Olin et al.

Title Page

Abstract

Introduction

Conclusions

References

Tables

Figures

◀

▶

◀

▶

Back

Close

Full Screen / Esc

Printer-friendly Version

Interactive Discussion

In A cases with $n_{sa} = 1$, only 0.5–4% of sulfuric acid condensed onto the particle phase (Table 2), but in R cases with $n_{sa} = 0.25$, about 80% condensed. The difference is caused by the condensation sinks of solid particles, mainly due to soot mode. Table 3 presents the composition of the liquid parts in the particles, which are in agreement with the results of Pirjola et al. (2014), with the exception of the water content, which is approximately the half of the water content in the results of Pirjola et al. (2014). Hydrocarbons dominate the particle mass in the cases of lower raw exhaust sulfuric acid concentrations. Table 3 also shows the maximum saturation vapor pressures of the hydrocarbons that are condensed onto the gas phase. The values correspond to low-volatile or semi-volatile organic compounds.

In reality, the shape of the region of highest nucleation rates would be different and probably transferred towards the inner wall of the sampling pipe of PTD due to the cooling of exhaust gas by dilution air that is not modeled here. DBP nucleation simulations of Pyykönen et al. (2007) show that nucleation occurs in two regions: (1) right before the perforated section, and (2) during the perforated section. If nucleation exponents are higher in reality, nucleation rate will diminish steeply in PTD region; therefore, the major part of nucleation will occur in PTD region. This could be examined by measuring particle concentrations inside the aging chamber or with aging chambers of different lengths. If the major part of nucleation occurs in the aging chamber, it is not obvious that the nucleation process will be stopped inside the secondary dilution. The position of nucleation region is also dependent on the effects of T and RH, but they cannot be observed from these simulations. Further investigations, where T and RH will be changed and particle concentration will be measured, are required to examine the influence of them.

4.2 Comparison between Eulerian and Lagrangian models

A simulation performed by the Eulerian model of A case with raw exhaust sulfuric acid concentration of $4.6 \times 10^{10} \text{ cm}^{-3}$ and with the nucleation exponent $n_{sa} = 1$ was modeled with the Lagrangian model also. The simulations was done on three path

CFD modeling of sulfur driven nucleation and growth in diluting diesel exhaust

M. Olin et al.

Title Page

Abstract

Introduction

Conclusions

References

Tables

Figures

◀

▶

◀

▶

Back

Close

Full Screen / Esc

Printer-friendly Version

Interactive Discussion

lines shown in Fig. 10, from which temperature profile and gas and particle dilution profiles as a function of time were exported from the CFD model. The blue path starts near the inner wall of the sampling tube, the red path near the axis, and the green path between them. Due to cylindrical symmetry, the blue path has the highest relevance on the output particle flux and the red path the lowest. All the three lines have the total residence time of about 1.6 s. The time domain was divided to 10^6 time steps, which corresponds to a higher resolution compared to the Eulerian simulation, where the paths pass through 6000–8000 computational cells.

Figure 11 presents the nucleation rates and the particle concentrations on the three path lines. The nucleation rate on the blue path develops slower compared to the green and the red paths. That is because the blue path travels near the wall, thus the velocity is lower due to friction, and 21 ms is required to reach the mixing region, which is a longer time than for the red (7 ms) and the green (8 ms) paths. In fact, the nucleation rate on the blue path develops fastest in spatial coordinates; because the blue path is the nearest path to the boundary where hot exhaust and cold dilution air encounter, where nucleation rate has the highest values.

Comparing the particle concentrations between the Eulerian and the Lagrangian simulations, it can be observed that the concentrations in the Eulerian simulations are higher in the beginning. That is caused by the diffusion of the particles from the surrounding areas of a path, which cannot be modeled with the Lagrangian model but is modeled in the Eulerian model. The highest particle concentrations are on the cold side of the blue path; hence, the diffusion transports particles onto the location of the three paths. However, the difference of the concentrations can also be partially accounted for numerical error caused by the lower resolution in the Eulerian simulation. The concentrations at the ends of all the paths are, however, almost the same, except for 20 % higher values in the Eulerian simulation. The concentrations develop to same values, because the major part of the nucleation occurs in the aging chamber where every path experiences almost the same nucleation rates.

CFD modeling of sulfur driven nucleation and growth in diluting diesel exhaust

M. Olin et al.

Title Page

Abstract

Introduction

Conclusions

References

Tables

Figures

◀

▶

◀

▶

Back

Close

Full Screen / Esc

Printer-friendly Version

Interactive Discussion



It can be seen from Fig. 12 that some numerical error exists at the time when nucleation starts in the Eulerian simulation, which can be seen as a noise in CMD and GSD values. In the case of the Lagrangian simulation, these values develop more smoothly through the time domain. The same time delay of the values on the blue path as for the nucleation rate can also be seen for CMD and GSD values. Due to the diffusion in the Eulerian simulation that mixes particles of different size from the surrounding areas of the paths with the path areas, the particle distributions become wider, which can be seen as increased GSD values compared to the values from the Lagrangian simulation. At the end, all GSD values approach the same value, but CMD values appear to be about 0.5 nm lower in the Lagrangian simulation during the whole time domain.

The Lagrangian model appear to produce almost equal results compared to the Eulerian model, if the output particle distribution is of interest only, despite the path line chosen to be simulated. It can be executed with very high time resolution without being computationally expensive. However, it requires cooling and dilution profiles obtained from the CFD model, if proper results are required. Additionally, the coupling of the fluid species with the aerosol dynamics is required to be modeled if the aerosol processes are limited by the concentrations of the gases, not by time.

Conversely, the Eulerian model can produce more detailed spatial information compared to the Lagrangian model, and the diffusion is also included in simulations. However, it is computationally more expensive; and therefore, the spatial resolution may remain too low.

4.3 Dependence of volatile nucleation mode concentration on sulfuric acid concentration

It can be seen from Fig. 13 that the nucleation exponent $n_{sa} = 0.25$ fits better for R cases and the nucleation exponent $n_{sa} = 1$ better for A cases. The nucleation exponent 0.25 could also fit to A cases equally well in the sulfuric acid concentration range between 2×10^{10} and $3 \times 10^{11} \text{ cm}^{-3}$. For R cases, there is also one measurement point with the lowest concentration that fits well with the nucleation exponent 1.

CFD modeling of sulfur driven nucleation and growth in diluting diesel exhaust

M. Olin et al.

Title Page

Abstract

Introduction

Conclusions

References

Tables

Figures

◀

▶

◀

▶

Back

Close

Full Screen / Esc

Printer-friendly Version

Interactive Discussion

However, there could have been underestimated particle concentrations with the lowest sulfuric acid concentrations in A cases, because the particle sizes were very low (~ 4 nm) for particle measurement devices. That underestimation was modeled by calculating the particles larger than 3.6 nm only (green lines in Fig. 13), which is the cut-size D_{50} of used particle counter TSI CPC 3025, according to Mordas et al. (2008). This decreased the concentrations and increased the slope of concentration very slightly, which is not enough for the nucleation exponent 0.25 to fit in all A cases. However, measured particle size data from A cases are not available. Additionally, particle losses inside the particle measurement setup and devices increase with decreasing particle size; thus the measured particle concentrations can then be underestimated even more.

The nucleation exponent n_{sa} can be estimated directly from the measurement data through the slope of N_{vol} vs. $[H_2SO_4]$, which are also 0.25 and 1. It is not always possible to estimate the nucleation exponent in this manner, because particle number concentration is not only dependent on nucleation rate, but on other aerosol processes too. Condensation and coagulation sinks have effects on the number concentration, especially for the case where soot particles exist, due to increased sinks. In these cases, the sinks resulting from solid particles were not sufficient to cause the slope to differ from the nucleation exponent, although about 77 % of sulfuric acid was condensed onto the solid particles. The effect of the sinks can be seen by comparing the particle number concentration levels in Fig. 13, where R cases have lower values compared to A cases. However, the soot particle sinks can be underestimated, because soot particles were modeled as spherical particles, which have different particle surface area compared to fractal particles.

For these cases, the nucleation exponents n_{sa} between 0.25 and 1 seem to produce the best results. Due to low nucleation exponents, it is probable that there are other compounds, such as low-volatile hydrocarbons, that account in the nucleation process. More realistic nucleation exponents may be obtained if a separate nucleation

mechanism for hydrocarbon nucleation is modeled, e.g., type of

$$J = K_1[\text{H}_2\text{SO}_4]^2 + K_2[\text{H}_2\text{SO}_4][\text{org}], \quad (14)$$

where [org] is some organics accounting in nucleation, has provided the most reliable results compared to BHN, activation, or kinetic nucleation (Pirjola et al., 2014). Validating attempts to model organic nucleation in vehicle exhaust would need both sulfuric acid and comprehensive hydrocarbon measurements in raw exhaust with particle distribution measurements.

The reason for different nucleation exponents between A and R cases is not obvious, and further research is required to examine that. The difference could be accounted for different sulfuric acid concentration range, different particle size range, or another reason that cannot be seen from the measurements or the simulations studied here. Sulfuric acid concentration range could cause the difference if the nucleation exponent were dependent on the sulfuric acid concentration in a way that the nucleation exponent decreases with increasing sulfuric acid concentration, which is actually seen in CNT. Different particle size range could explain the difference due to decreased counting efficiency with decreasing particle size; particle sizes were lower in A cases compared to R cases.

5 Conclusions

CFD-TUTEAM model was used to simulate particle formation process in the laboratory-scale diesel exhaust sampling system. A porous tube type diluter and an aging chamber were modeled as the sampling system. Eulerian and Lagrangian type sub-models were used, and the both models produced almost the same particle distributions at the outlet of the aging chamber. The Lagrangian model is computationally less expensive compared to the Eulerian model; thus, it can be modeled with a very high temporal resolution. However, cooling and dilution profiles from the Eulerian model are required

CFD modeling of sulfur driven nucleation and growth in diluting diesel exhaust

M. Olin et al.

Title Page

Abstract

Introduction

Conclusions

References

Tables

Figures

◀

▶

◀

▶

Back

Close

Full Screen / Esc

Printer-friendly Version

Interactive Discussion

as inputs for the Lagrangian model. Conversely, the Eulerian model produced more detailed spatial information inside the sampling system and it includes diffusion modeling. The main advantage of the modal aerosol model is that it can be used to examine particle formation spatially with lower computational cost compared to sectional aerosol models. The drawback of it relates to the assumption that the particle distributions remain log-normal, which is not true especially when nucleation and condensation occur simultaneously.

The highest nucleation rates were found to exist in the region where hot exhaust and cold dilution air encounter. However, due to low dilution ratio and low nucleation exponents, the nucleation rate remains high in the aging chamber, where the dilution process is already finished. Hence, the major part (over 99 %) of the volatile nucleation mode particles was formed in the aging chamber. With a higher nucleation exponent, the nucleation rate would diminish more steeply in the dilution region; thus, the major part of nucleation would occur in the diluter. Additional experimental data for examining the nucleation exponent could be obtained by measuring particle concentrations inside the aging chamber or with aging chambers of different lengths. If nucleation exponents are low in reality, the major part of nucleation will occur in the aging chamber; therefore, it is not obvious that the nucleation process will be stopped inside the secondary dilution.

The nucleation exponents for sulfuric acid in the range from 0.25 to 1 appeared to fit best with the measurement data, according to the simulations. In this range of condensation and coagulation sinks resulting from solid particles, the nucleation exponents can be estimated directly from the measurement data through the slope of the volatile nucleation mode number concentration vs. the raw exhaust sulfuric acid concentration. Due to the nucleation exponents below unity, it is probable that there are other compounds, such as organics, which affect on the nucleation rate. The reason for different nucleation exponents between the cases is not obvious, and further research is required to examine that.

CFD modeling of sulfur driven nucleation and growth in diluting diesel exhaust

M. Olin et al.

Title Page

Abstract

Introduction

Conclusions

References

Tables

Figures

◀

▶

◀

▶

Back

Close

Full Screen / Esc

Printer-friendly Version

Interactive Discussion



According to the simulations, the major part of deposition occurs in the region of the expander of the aging chamber. Turbulence increases in the expander, which increases the effective diffusion coefficient; and therefore, deposition rate increases. The expander had higher influence on core and soot mode compared to volatile nucleation mode, because the major part of the volatile nucleation mode particles was formed after the expander.

Appendix A: Detailed description of condensation modeling

A1 Mass growth rate equation

Modeled particle diameters are in the range from a molecule diameter to below 1 μm . This range participates in free-molecular, transition, and continuum regions. The Fuchs–Sutugin correction factor β_i (Seinfeld and Pandis, 2006) in the growth rate equation allows smooth behavior of condensation in all the regions. Especially for hydrocarbons, the growth rate calculation requires the molecule diameter d_i with very small particles, which is included in the equation as $(d_p + d_i)$ (Lehtinen and Kulmala, 2003).

The mass growth rate of a single particle in mode j by a condensing gas i becomes

$$\frac{\partial m_{p,j,i}}{\partial t} = \frac{2\pi m_i}{k_B T} (d_p + d_i) \beta_i (D_{p,\text{lam}} + D_{i,\text{lam}}) (\rho_i - \rho_{i,p}), \quad (\text{A1})$$

where m_i , $D_{i,\text{lam}}$, ρ_i , and $\rho_{i,p}$ are the molecule mass, diffusion coefficient, partial pressure, and vapor pressure on the particle surface of a gas i , respectively. For water and sulfuric acid, $\rho_{i,p}$ is calculated by

$$\rho_{i,p} = \frac{A_{\text{sa-w}}}{A_p} \Gamma_i K_i \rho_i^\circ, \quad (\text{A2})$$

where $A_{\text{sa-w}}$ is the surface area of sa-w phase in a particle, and A_p is the surface area of the whole particle. Γ_i , K_i , ρ_i° are activity (Taleb et al., 1996), Kelvin factor, and saturation

vapor pressure of gas i . For hydrocarbons, the last term of Eq. (A1) is computed as

$$(\rho_i - \rho_{i,p}) = f_{hc} \rho_{hc}. \quad (A3)$$

Kelvin factor for water and sulfuric acid is calculated by

$$K_i = \exp\left(\frac{4\sigma_{sa-w}m_i}{k_B T \rho_{sa-w} d_p}\right), \quad (A4)$$

- 5 where σ_{sa-w} and ρ_{sa-w} are surface tension (Vehkamäki et al., 2003) and density (Vehkamäki et al., 2002) of sa-w solution.

A2 Phase interactions

Liquid parts in particles are considered two immiscible phases: sulfuric acid-water phase (sa-w) and hydrocarbon (hc) phase. The phase with lower volume fraction is assumed to form a lens on the surface of the hydrocarbon phase (Ziemann and Mc-Murry, 1998) as shown in Fig. 2. The surface area of the whole particle A_p is considered the area onto which condensation occurs, regardless of the particle composition. However e.g., sulfuric acid does not evaporate from a particle from the area of hc phase. Therefore, the fraction $\frac{A_{sa-w}}{A_p}$ is used in Eq. (A2). The fraction can be obtained from geometrical calculations, and the following fitting functions are used as it:

$$\frac{A_{minor}}{A_p} = 0.237 \left(\frac{V_{minor}}{V_p}\right) + 0.539 \left(\frac{V_{minor}}{V_p}\right)^{\frac{1}{2}} \quad (A5)$$

for volatile nucleation mode. Subscript minor presents the phase with the minority of the volume V in the particle. For core mode, the fraction is

$$\frac{A_{minor}}{A_p} = 0.237 \left[\frac{V_{minor}}{V_p} (1 - d'^3)\right] + 0.539 \left[\frac{V_{minor}}{V_p} (1 - d'^3)\right]^{\frac{1}{2}} \quad (A6)$$

2930

Title Page

Abstract

Introduction

Conclusions

References

Tables

Figures

◀

▶

◀

▶

Back

Close

Full Screen / Esc

Printer-friendly Version

Interactive Discussion



if

$$\frac{V_{\text{minor}}}{V_p} < \frac{(1 - d')^2 (2 + d')}{4(1 - d'^3)} \quad (\text{A7})$$

and

$$\frac{A_{\text{minor}}}{A_p} = (0.336d'^{1.602} + 0.667) \left(\frac{V_{\text{minor}}}{V_p} \right) - 0.168d'^{1.602} + 0.167 \quad (\text{A8})$$

- 5 otherwise. In the equation, $d' = \frac{d_{\text{core}}}{d_p}$, where d_{core} denotes the solid core diameter in the nonvolatile nucleation mode particle. Due to more complex geometry of soot particles, a constant value of unity for the fraction is used for soot mode.

A3 Fraction of condensing hydrocarbons

10 Due to a wide range of different hydrocarbons in diesel exhaust, it is not reasonable to model them all. A new method to model hydrocarbons is implemented in the model. According to Donahue et al. (2006), hydrocarbons in diesel exhaust can be partitioned to bins with different volatilities. Hydrocarbons with partial pressure over corresponding vapor pressure on the particle are considered the fraction that is able to condense onto the particle phase. These hydrocarbons satisfy the equation

$$15 \rho_{\text{hc}} > \frac{A_{\text{hc}}}{A_p} \Gamma_{\text{hc}} \rho_{\text{hc}}^{\circ}(T), \quad (\text{A9})$$

where Kelvin factor calculation is neglected due to a wide range of the properties of different hydrocarbons. Unity is used as a value for activity of hydrocarbons Γ_{hc} .

Assuming the diesel exhaust organic aerosol volatility distribution measured by May et al. (2013), with a temperature T in Kelvins and partial pressure of total hydrocarbons

A4 Water equilibrium computation procedure

A particle in water equilibrium is defined as a particle onto which no condensation and from which no evaporation of water occurs. Therefore, the following equation is satisfied:

$$RH = \frac{A_{sa-w}}{A_p}(T, Y^{eq}) \Gamma_w(T, Y^{eq}) K_w(T, Y^{eq}, d_p), \quad (A12)$$

where Y^{eq} denotes the particle composition in water equilibrium.

The factor for water equilibrium κ_j in Eq. (8) is altered after every iteration of CFD software until volatile and nonvolatile nucleation mode particles in the whole computational domain are in water equilibrium. Ensuring water equilibrium is performed by checking that the particles satisfy Eq. (A12). Initially $\kappa_j = 1$, thus the composition Y^{eq} solved from Eq. (A12) is used to obtain an initial guess for the iterative procedure of water equilibrium.

For the Lagrangian model, water equilibrium is maintained by altering water content in the particles artificially after every time step in a way that Eq. (A12) is satisfied.

Acknowledgements. This work was funded by the Maj and Tor Nessling foundation (project number 2014452), by the Finnish Funding Agency for Technology and Innovation, Tekes (TREAM project), and by Dinex Ecocat Oy, Neste Oil Oy, AGCO Power, and Ab Nanol Technologies Oy.

References

- Albriet, B., Sartelet, K., Lacour, S., Carissimo, B., and Seigneur, C.: Modelling aerosol number distributions from a vehicle exhaust with an aerosol CFD model, *Atmos. Environ.*, 44, 1126–1137, doi:10.1016/j.atmosenv.2009.11.025, 2010. 2908, 2912
- Alföldy, B., Giechaskiel, B., Hofmann, W., and Drossinos, Y.: Size-distribution dependent lung deposition of diesel exhaust particles, *J. Aerosol Sci.*, 40, 652–663, doi:10.1016/j.jaerosci.2009.04.009, 2009. 2907

CFD modeling of sulfur driven nucleation and growth in diluting diesel exhaust

M. Olin et al.

Title Page

Abstract

Introduction

Conclusions

References

Tables

Figures

◀

▶

◀

▶

Back

Close

Full Screen / Esc

Printer-friendly Version

Interactive Discussion



- Hinds, W. C.: Aerosol Technology: Properties, Behavior, and Measurement of Airborne Particles, 2nd edn., John Wiley and Sons, Inc., Hoboken, USA, 1999. 2915
- Huang, L., Gong, S. L., Gordon, M., Liggio, J., Staebler, R., Stroud, C. A., Lu, G., Mihele, C., Brook, J. R., and Jia, C. Q.: Aerosol–computational fluid dynamics modeling of ultrafine and black carbon particle emission, dilution, and growth near roadways, *Atmos. Chem. Phys.*, 14, 12631–12648, doi:10.5194/acp-14-12631-2014, 2014. 2908, 2912
- Johansson, C., Norman, M., and Gidhagen, L.: Spatial and temporal variations of PM₁₀ and particle number concentrations in urban air, *Environ. Monit. Assess.*, 127, 477–487, doi:10.1007/s10661-006-9296-4, 2007. 2906
- Kashchiev, D.: On the relation between nucleation work, nucleus size, and nucleation rate, *J. Chem. Phys.*, 76, 5098–5102, doi:10.1063/1.442808, 1982. 2912, 2920
- Keskinen, J. and Rönkkö, T.: Can real-world diesel exhaust particle size distribution be reproduced in the laboratory? A critical review, *J. Air Waste Manage.*, 60, 1245–1255, doi:10.3155/1047-3289.60.10.1245, 2010. 2916
- Kittelson, D.: Engines and nanoparticles: a review, *J. Aerosol Sci.*, 29, 575–588, doi:10.1016/S0021-8502(97)10037-4, 1998. 2907
- Kittelson, D., Watts, W., Johnson, J., Thorne, C., Higham, C., Payne, M., Goodier, S., Warrens, C., Preston, H., Zink, U., Pickles, D., Goersmann, C., Twigg, M., Walker, A., and Boddy, R.: Effect of fuel and lube oil sulfur on the performance of a diesel exhaust gas continuously regenerating trap, *Environ. Sci. Technol.*, 42, 9276–9282, doi:10.1021/es703270j, 2008. 2907
- Kulmala, M. and Laaksonen, A.: Binary nucleation of water-sulfuric acid system: Comparison of classical theories with different H₂SO₄ saturation vapor pressures, *J. Chem. Phys.*, 93, 696–701, doi:10.1063/1.459519, 1990. 2914
- Kulmala, M., Lehtinen, K. E. J., and Laaksonen, A.: Cluster activation theory as an explanation of the linear dependence between formation rate of 3nm particles and sulphuric acid concentration, *Atmos. Chem. Phys.*, 6, 787–793, doi:10.5194/acp-6-787-2006, 2006. 2912
- Kulmala, M., Riipinen, I., Sipilä, M., Manninen, H. E., Petäjä, T., Junninen, H., Dal Maso, M., Mordas, G., Mirme, A., Vana, M., Hirsikko, A., Laakso, L., Harrison, R. M., Hanson, I., Leung, C., Lehtinen, K. E. J., and Kerminen, V.-M.: Toward direct measurement of atmospheric nucleation, *Science*, 318, 89–92, doi:10.1126/science.1144124, 2007. 2920
- Kupiainen-Määttä, O., Olenius, T., Korhonen, H., Malila, J., Dal Maso, M., Lehtinen, K., and Vehkamäki, H.: Critical cluster size cannot in practice be determined by

CFD modeling of sulfur driven nucleation and growth in diluting diesel exhaust

M. Olin et al.

Title Page

Abstract

Introduction

Conclusions

References

Tables

Figures

◀

▶

◀

▶

Back

Close

Full Screen / Esc

Printer-friendly Version

Interactive Discussion



- McMurry, P. and Friedlander, S.: New particle formation in the presence of an aerosol, *Atmos. Environ.*, 13, 1635–1651, doi:10.1016/0004-6981(79)90322-6, 1979. 2912
- Mordas, G., Manninen, H., Petäjä, T., Aalto, P., Hämeri, K., and Kulmala, M.: On operation of the ultra-fine water-based CPC TSI 3786 and comparison with other TSI models (TSI 3776, TSI 3772, TSI 3025, TSI 3010, TSI 3007), *Aerosol Sci. Tech.*, 42, 152–158, doi:10.1080/02786820701846252, 2008. 2926
- Ntziachristos, L., Giechaskiel, B., Pistikopoulos, P., Samaras, Z., Mathis, U., Mohr, M., Ristimäki, J., Keskinen, J., Mikkanen, P., Casati, R., Scheer, V., and Vogt, R.: Performance evaluation of a novel sampling and measurement system for exhaust particle characterization, *SAE Tech. Paper Ser.*, 2004-01-1439, doi:10.4271/2004-01-1439, 2004. 2916
- Olin, M., Dal Maso, M., and Rönkkö, T.: Sulfur driven nucleation in diesel exhaust: simulations of a laboratory sampling system, in: *Proceedings of the 18th ETH-Conference on Combustion Generated Nanoparticles*, Zürich, Switzerland, 22–25 June 2014, 45–46, 2014. 2912, 2920, 2944
- Paasonen, P., Nieminen, T., Asmi, E., Manninen, H. E., Petäjä, T., Plass-Dülmer, C., Flen-tje, H., Birmili, W., Wiedensohler, A., Hörrak, U., Metzger, A., Hamed, A., Laaksonen, A., Facchini, M. C., Kerminen, V.-M., and Kulmala, M.: On the roles of sulphuric acid and low-volatility organic vapours in the initial steps of atmospheric new particle formation, *Atmos. Chem. Phys.*, 10, 11223–11242, doi:10.5194/acp-10-11223-2010, 2010. 2912, 2913
- Pey, J., Querol, X., Alastuey, A., Rodriguez, S., Putaud, J., and Van Dingenen, R.: Source apportionment of urban fine and ultra-fine particle number concentration in a Western Mediterranean city, *Atmos. Environ.*, 43, 4407–4415, doi:10.1016/j.atmosenv.2009.05.024, 2009. 2906
- Pirjola, L., Karl, M., Rönkkö, T., and Arnold, F.: Model studies on the formation of volatile diesel exhaust particles: are organic vapours involved in nucleation and growth?, submitted to *Atmos. Chem. Phys. Discuss.*, 2014. 2908, 2923, 2927
- Pope, C., Burnett, R., Thun, M., Calle, E., Krewski, D., Ito, K., and Thurston, G.: Lung cancer, cardiopulmonary mortality, and long-term exposure to fine particulate air pollution, *J. Amer. Med. Assoc.*, 287, 1132–1141, doi:10.1001/jama.287.9.1132, 2002. 2906
- Pyykönen, J., Miettinen, M., Sippula, O., Leskinen, A., Raunemaa, T., and Jokiniemi, J.: Nucleation in a perforated tube diluter, *J. Aerosol Sci.*, 38, 172–191, doi:10.1016/j.jaerosci.2006.11.006, 2007. 2908, 2923

CFD modeling of sulfur driven nucleation and growth in diluting diesel exhaust

M. Olin et al.

Title Page

Abstract

Introduction

Conclusions

References

Tables

Figures

◀

▶

◀

▶

Back

Close

Full Screen / Esc

Printer-friendly Version

Interactive Discussion



- Rissler, J., Swietlicki, E., Bengtsson, A., Boman, C., Pagels, J., Sandström, T., Blomberg, A., and Löndahl, J.: Experimental determination of deposition of diesel exhaust particles in the human respiratory tract, *J. Aerosol Sci.*, 48, 18–33, doi:10.1016/j.jaerosci.2012.01.005, 2012. 2907
- 5 Rönkkö, T., Virtanen, A., Vaaraslahti, K., Keskinen, J., Pirjola, L., and Lappi, M.: Effect of dilution conditions and driving parameters on nucleation mode particles in diesel exhaust: laboratory and on-road study, *Atmos. Environ.*, 40, 2893–2901, doi:10.1016/j.atmosenv.2006.01.002, 2006. 2913
- Rönkkö, T., Virtanen, A., Kannosto, J., Keskinen, J., Lappi, M., and Pirjola, L.: Nucleation mode particles with a nonvolatile core in the exhaust of a heavy duty diesel vehicle, *Environ. Sci. Technol.*, 41, 6384–6389, doi:10.1021/es0705339, 2007. 2907, 2908
- 10 Rönkkö, T., Lähde, T., Heikkilä, J., Pirjola, L., Bauschke, U., Arnold, F., Schlager, H., Rothe, D., Yli-Ojanperä, J., and Keskinen, J.: Effects of gaseous sulphuric acid on diesel exhaust nanoparticle formation and characteristics, *Environ. Sci. Technol.*, 47, 11882–11889, doi:10.1021/es402354y, 2013. 2907, 2908, 2916, 2917, 2918, 2952, 2956
- 15 Sakurai, H., Tobias, H., Park, K., Zarling, D., Docherty, K., Kittelson, D., McMurry, P., and Ziemann, P.: On-line measurements of diesel nanoparticle composition and volatility, *Atmos. Environ.*, 37, 1199–1210, doi:10.1016/S1352-2310(02)01017-8, 2003. 2907
- Schauer, J., Kleeman, M., Cass, G., and Simoneit, B.: Measurement of emissions from air pollution sources. 2. C1 through C30 organic compounds from medium duty diesel trucks, *Environ. Sci. Technol.*, 33, 1578–1587, doi:10.1021/es980081n, 1999. 2932
- 20 Schneider, J., Hock, N., Weimer, S., Borrmann, S., Kirchner, U., Vogt, R., and Scheer, V.: Nucleation particles in diesel exhaust: composition inferred from in situ mass spectrometric analysis, *Environ. Sci. Technol.*, 39, 6153–6161, doi:10.1021/es049427m, 2005. 2907
- 25 Seinfeld, J. and Pandis, S.: *Atmospheric Chemistry and Physics: From Air Pollution to Climate Change*, 2nd edn., John Wiley and Sons, Inc., Hoboken, USA, 2006. 2929
- Sgro, L., Borghese, A., Speranza, L., Barone, A., Minutolo, P., Bruno, A., D’Anna, A., and D’Alessio, A.: Measurements of nanoparticles of organic carbon and soot in flames and vehicle exhausts, *Environ. Sci. Technol.*, 42, 859–863, doi:10.1021/es070485s, 2008. 2907
- 30 Sihto, S.-L., Vuollekoski, H., Leppä, J., Riipinen, I., Kerminen, V.-M., Korhonen, H., Lehtinen, K. E. J., Boy, M., and Kulmala, M.: Aerosol dynamics simulations on the connection of sulphuric acid and new particle formation, *Atmos. Chem. Phys.*, 9, 2933–2947, doi:10.5194/acp-9-2933-2009, 2009. 2912, 2913

CFD modeling of sulfur driven nucleation and growth in diluting diesel exhaust

M. Olin et al.

Title Page

Abstract

Introduction

Conclusions

References

Tables

Figures

◀

▶

◀

▶

Back

Close

Full Screen / Esc

Printer-friendly Version

Interactive Discussion



- Taleb, D.-E., Ponche, J.-L., and Mirabel, P.: Vapor pressures in the ternary system water-nitric acid-sulfuric acid at low temperature: a reexamination, *J. Geophys. Res.-Atmos.*, 101, 25967–25977, doi:10.1029/96JD02330, 1996. 2929
- 5 Tobias, H., Beving, D., Ziemann, P., Sakurai, H., Zuk, M., McMurry, P., Zarling, D., Waytulonis, R., and Kittelson, D.: Chemical analysis of diesel engine nanoparticles using a nano-DMA/thermal desorption particle beam mass spectrometer, *Environ. Sci. Technol.*, 35, 2233–2243, doi:10.1021/es0016654, 2001. 2907
- Uhrner, U., von Löwis, S., Vehkamäki, H., Wehner, B., Bräsel, S., Hermann, M., Stratmann, F., Kulmala, M., and Wiedensohler, A.: Dilution and aerosol dynamics within a diesel car exhaust plume-CFD simulations of on-road measurement conditions, *Atmos. Environ.*, 41, 7440–7461, doi:10.1016/j.atmosenv.2007.05.057, 2007. 2908, 2912, 2914
- 10 Vaaraslahti, K., Keskinen, J., Giechaskiel, B., Solla, A., Murtonen, T., and Vesala, H.: Effect of lubricant on the formation of heavy-duty diesel exhaust nanoparticles, *Environ. Sci. Technol.*, 39, 8497–8504, doi:10.1021/es0505503, 2005. 2907
- 15 Vehkamäki, H. and Riipinen, I.: Thermodynamics and kinetics of atmospheric aerosol particle formation and growth, *Chem. Soc. Rev.*, 41, 5160–5173, doi:10.1039/C2CS00002D, 2012. 2907, 2912
- Vehkamäki, H., Kulmala, M., Napari, I., Lehtinen, K., Timmreck, C., Noppel, M., and Laaksonen, A.: An improved parameterization for sulfuric acid-water nucleation rates for tropospheric and stratospheric conditions, *J. Geophys. Res.-Atmos.*, 107, AAC 3–1–AAC 3–10, doi:10.1029/2002JD002184, 2002. 2930
- 20 Vehkamäki, H., Kulmala, M., Lehtinen, K., and Noppel, M.: Modelling binary homogeneous nucleation of water-sulfuric acid vapours: parameterisation for high temperature emissions, *Environ. Sci. Technol.*, 37, 3392–3398, doi:10.1021/es0263442, 2003. 2930
- 25 Virtanen, A., Ristimäki, J., Marjamäki, M., Vaaraslahti, K., Keskinen, J., and Lappi, M.: Effective density of diesel exhaust particles as a function of size, *SAE Tech. Paper Ser.*, 2002-01-0056, doi:10.4271/2002-01-0056, 2002. 2919
- Virtanen, A., Rönkkö, T., Kannosto, J., Ristimäki, J., Mäkelä, J. M., Keskinen, J., Pakkanen, T., Hillamo, R., Pirjola, L., and Hämeri, K.: Winter and summer time size distributions and densities of traffic-related aerosol particles at a busy highway in Helsinki, *Atmos. Chem. Phys.*, 6, 2411–2421, doi:10.5194/acp-6-2411-2006, 2006. 2906
- 30

CFD modeling of sulfur driven nucleation and growth in diluting diesel exhaust

M. Olin et al.

Title Page

Abstract

Introduction

Conclusions

References

Tables

Figures

◀

▶

◀

▶

Back

Close

Full Screen / Esc

Printer-friendly Version

Interactive Discussion

- Vogt, R., Scheer, V., Casati, R., and Benter, T.: On-road measurement of particle emission in the exhaust plume of a diesel passenger car, *Environ. Sci. Technol.*, 37, 4070–4076, doi:10.1021/es0300315, 2003. 2907
- 5 Vouitsis, E., Ntziachristos, L., and Samaras, Z.: Modelling of diesel exhaust aerosol during laboratory sampling, *Atmos. Environ.*, 39, 1335–1345, doi:10.1016/j.atmosenv.2004.11.011, 2005. 2908
- Wang, Y. and Zhang, K.: Coupled turbulence and aerosol dynamics modeling of vehicle exhaust plumes using the CTAG model, *Atmos. Environ.*, 59, 284–293, doi:10.1016/j.atmosenv.2012.04.062, 2012. 2908, 2912
- 10 Whitby, E. and McMurry, P.: Modal aerosol dynamics modeling, *Aerosol Sci. Tech.*, 27, 673–688, doi:10.1080/02786829708965504, 1997. 2909, 2910, 2915
- Wilck, M.: Modal modelling of multicomponent aerosols, Ph. D. thesis, Universität Leipzig, Leipzig, Germany, 1998. 2914
- 15 Ziemann, P. J. and McMurry, P. H.: Secondary electron yield measurements as a means for probing organic films on aerosol particles, *Aerosol Sci. Tech.*, 28, 77–90, doi:10.1080/02786829808965513, 1998. 2930

CFD modeling of sulfur driven nucleation and growth in diluting diesel exhaust

M. Olin et al.

Table 1. Boundary conditions for the simulations.

Boundary	Temperature (°C)	sa mole fraction	w mole fraction	hc mole fraction (ppmC ₁)	Flow rate (SLPM)	N_{core} (cm ⁻³)	N_{soot} (cm ⁻³)
Exhaust inlet	~ 430	7×10^{-11} – 4×10^{-8} ^a	0.085	3–8.5 (fitted)	4.5	0 – 5×10^6	0 – 4×10^6
Dilution air inlet	~ 30	0	~ 0.004 (10 %RH)	0	50	0	0
Inner walls	Coupled	Zero flux ^b	0 ^c or zero flux ^b	0 ^c or zero flux ^b	0	0	0

^a Corresponds to 7×10^8 – 4×10^{11} cm⁻³.

^b If saturation ratio is below unity, gas is not depositing.

^c If saturation ratio is over unity, gas is depositing.

Title Page

Abstract

Introduction

Conclusions

References

Tables

Figures

◀

▶

◀

▶

Back

Close

Full Screen / Esc

Printer-friendly Version

Interactive Discussion



CFD modeling of sulfur driven nucleation and growth in diluting diesel exhaust

M. Olin et al.

Title Page

Abstract

Introduction

Conclusions

References

Tables

Figures

◀

▶

◀

▶

Back

Close

Full Screen / Esc

Printer-friendly Version

Interactive Discussion

Table 2. Proportions of sulfuric acid found in different modes and remained in the gas phase (%) at the end of the aging chamber.

Mode	A, $n_{sa} = 1$	R, $n_{sa} = 0.25$
vol	0.5–4	0.2–4
soot	–	72–74
core	–	1.3–4.5
gas	96–99.5	19–22

CFD modeling of sulfur driven nucleation and growth in diluting diesel exhaust

M. Olin et al.

Title Page

Abstract

Introduction

Conclusions

References

Tables

Figures

◀

▶

◀

▶

Back

Close

Full Screen / Esc

Printer-friendly Version

Interactive Discussion



Table 3. Particle liquid part composition (mass-%) and the maximum saturation vapor pressures of hydrocarbons at the end of the aging chamber.

Mode	A, $n_{sa} = 1$			R, $n_{sa} = 0.25$		
	sa	w	hc	sa	w	hc
vol	2.4–14	0.5–8	77–97	0.6–9.4	0.14–6.2	84–99
soot	–	–	–	0.6–16	0.17–4.7	79–99
core	–	–	–	0.4–11	0.62–7.3	82–99
$p_{hc}^{\circ}(298\text{K})$	$< 5 \times 10^{-7}$ Pa			$< 5 \times 10^{-6} - < 2 \times 10^{-5}$ Pa		

CFD modeling of sulfur driven nucleation and growth in diluting diesel exhaust

M. Olin et al.

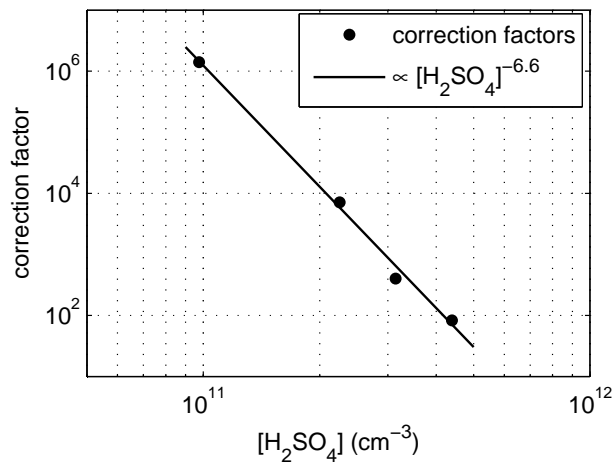


Figure 1. Correction factors for nucleation rate obtained from CNT as a function of raw exhaust sulfuric acid concentration. Figure adapted from Olin et al. (2014).

[Title Page](#)[Abstract](#)[Introduction](#)[Conclusions](#)[References](#)[Tables](#)[Figures](#)[◀](#)[▶](#)[◀](#)[▶](#)[Back](#)[Close](#)[Full Screen / Esc](#)[Printer-friendly Version](#)[Interactive Discussion](#)

CFD modeling of sulfur driven nucleation and growth in diluting diesel exhaust

M. Olin et al.

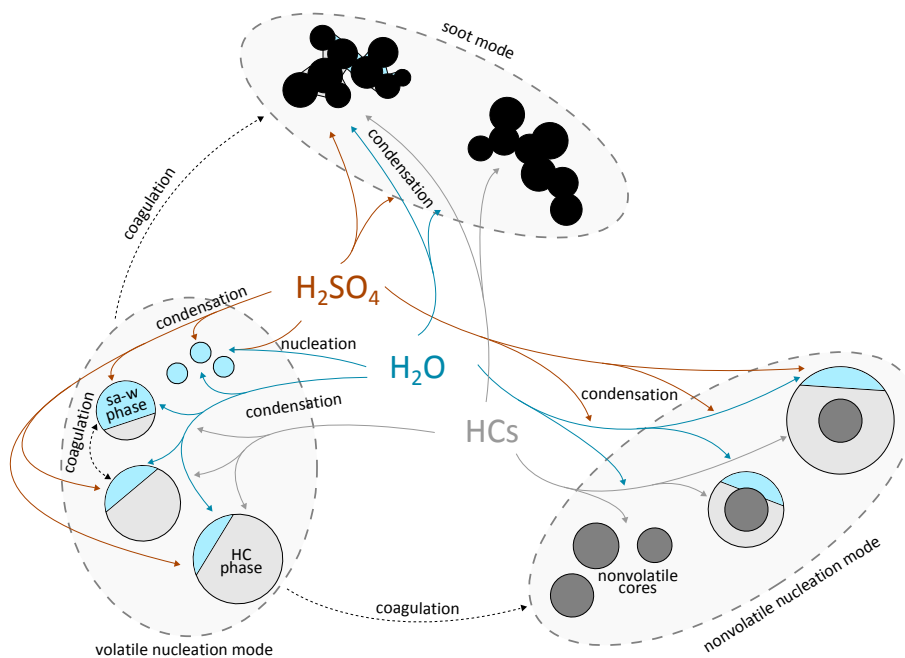


Figure 2. Modeled aerosol processes, modes, components, and phases. Detailed information on them are explained in Sect. 2.2.3 and in Appendix A.

Title Page

Abstract

Introduction

Conclusions

References

Tables

Figures

◀

▶

◀

▶

Back

Close

Full Screen / Esc

Printer-friendly Version

Interactive Discussion

CFD modeling of sulfur driven nucleation and growth in diluting diesel exhaust

M. Olin et al.

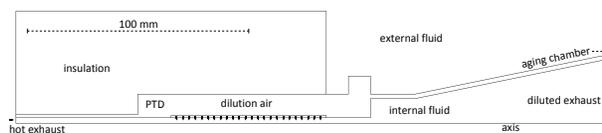


Figure 3. The upwind side of the computational domain. The geometry is axial symmetric, where the hot exhaust inlet is on the left, and the dilution air is supplied radially from a cylindrical boundary. The aging chamber continues towards right and it is 1 m of length. PTD is insulated but the latter part lies in stagnant external fluid.

[Title Page](#)[Abstract](#)[Introduction](#)[Conclusions](#)[References](#)[Tables](#)[Figures](#)[◀](#)[▶](#)[◀](#)[▶](#)[Back](#)[Close](#)[Full Screen / Esc](#)[Printer-friendly Version](#)[Interactive Discussion](#)

CFD modeling of sulfur driven nucleation and growth in diluting diesel exhaust

M. Olin et al.

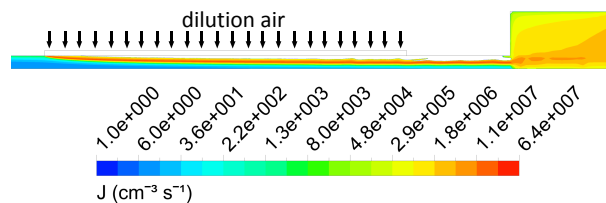


Figure 4. Nucleation rate in PTD region when $[\text{H}_2\text{SO}_4] = 1.47 \times 10^{11} \text{ cm}^{-3}$ in raw exhaust of R case with $n_{\text{sa}} = 0.25$.

[Title Page](#)[Abstract](#)[Introduction](#)[Conclusions](#)[References](#)[Tables](#)[Figures](#)[◀](#)[▶](#)[◀](#)[▶](#)[Back](#)[Close](#)[Full Screen / Esc](#)[Printer-friendly Version](#)[Interactive Discussion](#)

CFD modeling of sulfur driven nucleation and growth in diluting diesel exhaust

M. Olin et al.

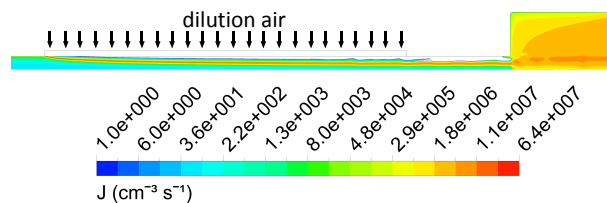


Figure 5. Nucleation rate in PTD region when $[\text{H}_2\text{SO}_4] = 1.47 \times 10^{11} \text{ cm}^{-3}$ in raw exhaust of R case with $n_{\text{sa}} = 1$.

Title Page

Abstract

Introduction

Conclusions

References

Tables

Figures

◀

▶

◀

▶

Back

Close

Full Screen / Esc

Printer-friendly Version

Interactive Discussion



CFD modeling of sulfur driven nucleation and growth in diluting diesel exhaust

M. Olin et al.

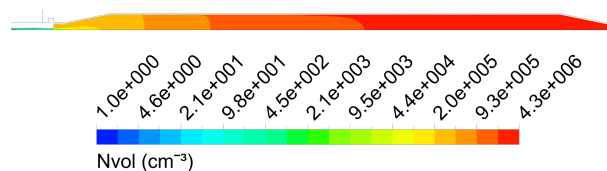


Figure 6. Volatile nucleation mode concentration in aging chamber region when $[\text{H}_2\text{SO}_4] = 1.47 \times 10^{11} \text{ cm}^{-3}$ in raw exhaust of R case with $n_{\text{sa}} = 0.25$.

[Title Page](#)[Abstract](#)[Introduction](#)[Conclusions](#)[References](#)[Tables](#)[Figures](#)[◀](#)[▶](#)[◀](#)[▶](#)[Back](#)[Close](#)[Full Screen / Esc](#)[Printer-friendly Version](#)[Interactive Discussion](#)

CFD modeling of sulfur driven nucleation and growth in diluting diesel exhaust

M. Olin et al.

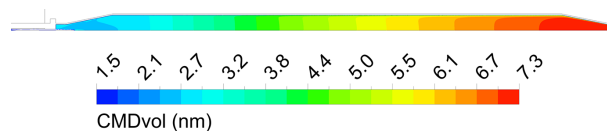


Figure 7. Volatile nucleation mode CMD in aging chamber region when $[\text{H}_2\text{SO}_4] = 1.47 \times 10^{11} \text{ cm}^{-3}$ in raw exhaust of R case with $n_{\text{sa}} = 0.25$.

Title Page

Abstract

Introduction

Conclusions

References

Tables

Figures

◀

▶

◀

▶

Back

Close

Full Screen / Esc

Printer-friendly Version

Interactive Discussion



CFD modeling of sulfur driven nucleation and growth in diluting diesel exhaust

M. Olin et al.

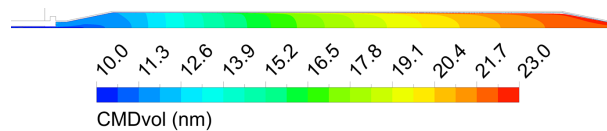


Figure 8. Core mode CMD in aging chamber region when $[\text{H}_2\text{SO}_4] = 1.47 \times 10^{11} \text{ cm}^{-3}$ in raw exhaust of R case with $n_{\text{sa}} = 0.25$.

[Title Page](#)[Abstract](#)[Introduction](#)[Conclusions](#)[References](#)[Tables](#)[Figures](#)[◀](#)[▶](#)[◀](#)[▶](#)[Back](#)[Close](#)[Full Screen / Esc](#)[Printer-friendly Version](#)[Interactive Discussion](#)

CFD modeling of sulfur driven nucleation and growth in diluting diesel exhaust

M. Olin et al.

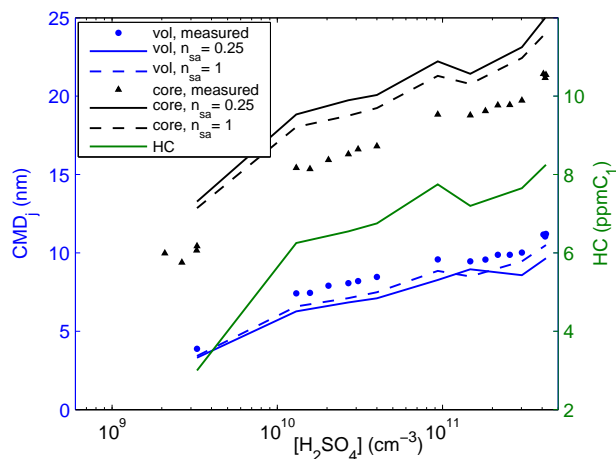


Figure 9. Measured and simulated CMD_{vol} and CMD_{core} and hydrocarbon amount in raw exhaust as a function of raw exhaust sulfuric acid concentration in R cases. Measurement data are obtained from Rönkkö et al. (2013).

Title Page

Abstract

Introduction

Conclusions

References

Tables

Figures

◀

▶

◀

▶

Back

Close

Full Screen / Esc

Printer-friendly Version

Interactive Discussion

CFD modeling of sulfur driven nucleation and growth in diluting diesel exhaust

M. Olin et al.

**Figure 10.** Path lines in PTD region for Lagrangian simulation.[Title Page](#)[Abstract](#)[Introduction](#)[Conclusions](#)[References](#)[Tables](#)[Figures](#)[Back](#)[Close](#)[Full Screen / Esc](#)[Printer-friendly Version](#)[Interactive Discussion](#)

CFD modeling of sulfur driven nucleation and growth in diluting diesel exhaust

M. Olin et al.

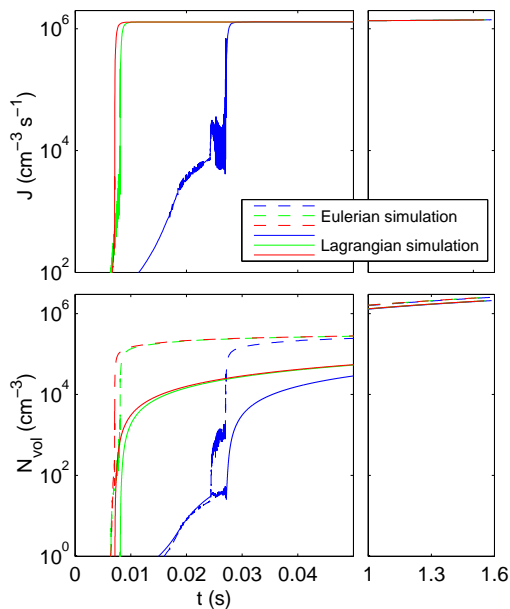


Figure 11. Nucleation rate and particle concentration as a function of time on three path lines. Nucleation rate profiles are the same in both simulations. The right plots present the ends of the paths.

CFD modeling of sulfur driven nucleation and growth in diluting diesel exhaust

M. Olin et al.

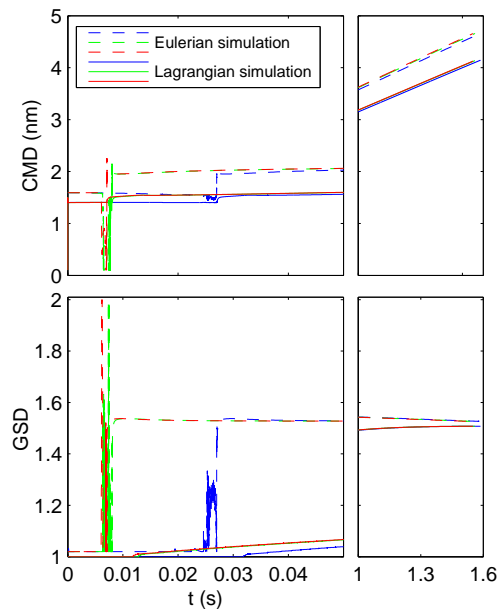


Figure 12. CMD_{vol} and GSD_{vol} as a function of time on three path lines. The right plots present the ends of the paths.

Title Page	
Abstract	Introduction
Conclusions	References
Tables	Figures
◀	▶
◀	▶
Back	Close
Full Screen / Esc	
Printer-friendly Version	
Interactive Discussion	



CFD modeling of sulfur driven nucleation and growth in diluting diesel exhaust

M. Olin et al.

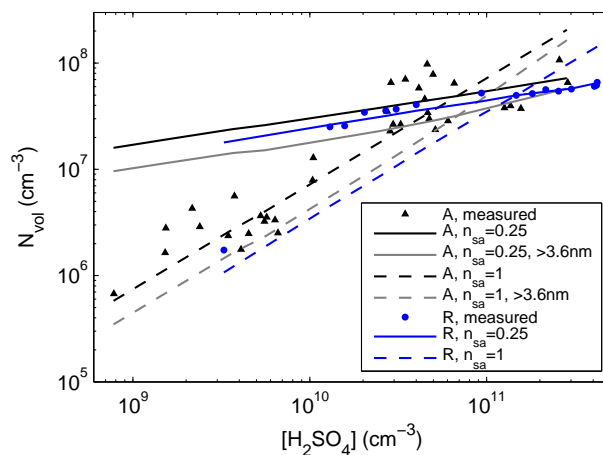


Figure 13. Measured and simulated volatile nucleation mode concentrations as a function of raw exhaust sulfuric acid concentration. Particle concentrations are normalized to raw exhaust by dilution ratio 12. Measurement data for R cases are obtained from Rönkkö et al. (2013) and for A cases from Arnold et al. (2012).

Title Page

Abstract

Introduction

Conclusions

References

Tables

Figures

◀

▶

◀

▶

Back

Close

Full Screen / Esc

Printer-friendly Version

Interactive Discussion